THE JOURNAL OF PHYSICAL CHEMISTRY B

Article

pubs.acs.org/JPCB

A Novel Tri-Enzyme System in Combination with Laser-Driven NMR Enables Efficient Nuclear Polarization of Biomolecules in Solution

Jung Ho Lee and Silvia Cavagnero*

Department of Chemistry and Biophysics Program, University of Wisconsin—Madison, 1101 University Avenue, Madison, Wisconsin 53706-1322, United States

Supporting Information

ABSTRACT: NMR is an extremely powerful, yet insensitive technique. Many available nuclear polarization methods that address sensitivity are not directly applicable to low-concentration biomolecules in liquids and are often too invasive. Photochemically induced dynamic nuclear polarization (photo-CIDNP) is no exception. It needs high-power laser irradiation, which often leads to sample degradation, and photosensitizer reduction. Here, we introduce a novel tri-enzyme system that significantly overcomes the above challenges, rendering photo-CIDNP a practically applicable technique for NMR sensitivity enhancement in solution. The specificity of the nitrate reductase (NR) enzyme is exploited to selectively *in situ* reoxidize the reduced photo-CIDNP dye $FMNH_2$. At the same time, the oxygen-scavenging ability of glucose oxidase (GO) and catalase (CAT) is synergistically employed to prevent sample photodegradation. The resulting tri-enzyme system (NR-GO-CAT) enables prolonged sensitivity-enhanced data collection in 1D and 2D heteronuclear NMR, leading to the highest photo-CIDNP sensitivity enhancement (48-fold relative to SE-HSQC) achieved to date for amino acids and polypeptides in solution. NR-GO-CAT extends the concentration limit of photo-CIDNP NMR down to the low micromolar range. In addition, sensitivity (relative to the reference SE-HSQC) is found to be inversely proportional to sample concentration, paving the way for the future analysis of even more diluted samples.

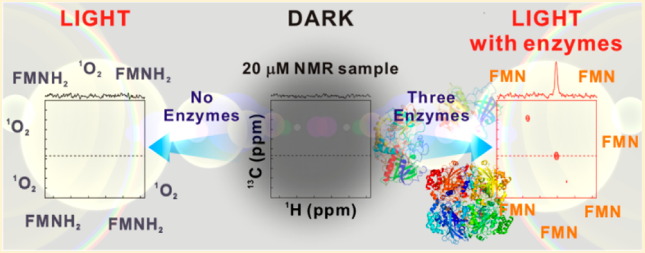

INTRODUCTION

Nuclear magnetic resonance (NMR) is arguably the most powerful technique to determine molecular structure and dynamics in solution at atomic resolution. On the other hand, NMR is intrinsically insensitive due to the similarity in nuclear spin populations of ground and excited states at thermal equilibrium, even in the presence of high applied magnetic fields. Major ongoing efforts in NMR spectroscopy aim at enhancing nuclear spin polarization in solids, liquids, and gases by approaches known as dynamic nuclear polarization (DNP),[1−3] dissolution-DNP,[4,5] parahydrogen-induced polarization (PHIP),[6,7] optical pumping,[8,9] Haupt effect,[10] and photochemically induced dynamic nuclear polarization (photo-CIDNP).[11−17] The latter technique, photo-CIDNP, is particularly attractive in the case of soluble biomolecules, as it can be used to increase NMR sensitivity under mild solution conditions.

Photo-CIDNP is typically carried out in the presence of a photosensitive dye capable of efficient intersystem crossing (e.g., flavin mononucleotide, also known as FMN) and transient substrate oxidation upon light excitation.[18,19] Sensitivity enhancements up to ca. 200-fold relative to the laser-free *dark* experiment have recently been achieved in solution for a variety of amino acids, peptides, and proteins via ^{13}C-PRINT, a ^{1}H-detected ^{13}C photo-CIDNP pulse sequence capable of enhancing the side chain and backbone resonances of Trp, His, and Tyr.[20] The photosynthetic reaction center, i.e., a large biomolecular complex susceptible to intramolecular light-induced electron transfer, can even yield ∼10 000-fold ^{13}C sensitivity enhancements.[21,22] Photo-CIDNP's primary advantages over other nuclear polarization approaches are the ability to operate under mild solution conditions and the relative simplicity of technical setup. Further, the use of this methodology for sensitivity enhancement purposes is still largely unexplored,[20,23−27] and holds potential for even larger enhancements upon optimization of dye structure, laser irradiation schemes, and other data collection parameters.

The inability to analyze low-concentration samples is one of the major limitations of NMR over other spectroscopies like fluorescence. As a result, typical NMR samples are limited to concentrations spanning from the hundreds of micromolar to the millimolar range. This is often a major limitation in biological and biomedical applications, where sample amounts are often scarce and poor solubility may impose additional low-concentration constraints.[28,29] The quest to increase NMR sensitivity is particularly pronounced in physiological environments, where low concentration and solubility are often matched by highly crowded media and intermolecular

Received: January 29, 2013
Revised: March 22, 2013
Published: April 5, 2013

interactions, which contribute to further increase resonance linewidths and decrease intensities. In the case of photo-CIDNP-induced highly polarized magnetization, prolonged signal averaging can potentially enable the analysis of very dilute samples, e.g., in the low-μM concentration range or lower, with significant improvements in signal-to-noise (S/N). In photo-CIDNP, however, three main challenges (Figure 1a) need to be overcome before this goal can be achieved. First, laser irradiation, especially at high power, leads to irreversible photodegradation of the target NMR sample, especially if it bears an aromatic moiety.[30,31] Second, laser irradiation also causes chemical damage of the dye.[32−34] Third, the dye, typically flavin mononucleotide (FMN), experiences reversible reduction (e.g., leading to $FMNH_2$) during photo-CIDNP.[34−36] The reduced dye then needs to be reoxidized so that subsequent rounds of photo-CIDNP can take place.

Previous efforts to facilitate long-term photo-CIDNP and address the above challenges include (a) deliberate modulation of the oxygen concentration in the sample,[30] (b) addition of the oxidizing agent H_2O_2 to the NMR sample to regenerate the yellow FMN dye from its photoreduced nearly colorless $FMNH_2$,[35] and (c) regeneration of FMN by mechanical mixing during the experiment to facilitate oxidation by ambient oxygen (Figure 1b).[35,37] Approach a leads to decreased photo-CIDNP regardless of whether oxygen is added or depleted. Specifically, under oxygen-saturation conditions, ^{T}FMN quenching prevents effective photo-CIDNP (Figure 1a). Under oxygen-depletion conditions, photodegradation is efficiently suppressed (Figure 1a) but the photoreduced $FMNH_2$ is not efficiently reoxidized to the original FMN (Figure 1b). Approaches b and c are effective. However, long-term photo-CIDNP data collection is not ideal in the presence of oxidizing agents such as H_2O_2 even if they act slowly (approach b), and sample disturbance during the experiment is generally undesirable (approach c). Moreover, the sample photodegradation problem is not addressed by approaches b and c.

Here, we introduce a novel tri-enzyme system capable of simultaneously tackling the sample photodegradation and $FMNH_2$ reoxidation challenges (Figure 1c). As shown in Figure 1d, the enzyme system comprises glucose oxidase (GO), catalase (CAT), and nitrate reductase (NR). This novel system has two complementary features. The oxygen scavenging component, which includes GO and CAT, prevents the singlet-oxygen-mediated sample degradation caused by the light-induced generation of ^{T}FMN (Figure 1a). In addition, the oxidizing component NR efficiently and specifically oxidizes $FMNH_2$ back to FMN in the absence of oxygen. NR is a molybdenum-containing enzyme known to catalyze the conversion of nitrate to nitrite in plants, algae, and fungi.[38] The tri-enzyme system (denoted here as NR-GO-CAT) extends the sample concentration limit of photo-CIDNP NMR down to the low micromolar range and greatly facilitates multidimensional photo-CIDNP applications while largely preserving substrate integrity.

EXPERIMENTAL METHODS

Enzyme Stock Solutions. Glucose oxidase (GO, from *Aspergillus niger*, catalog number G7141, Enzyme Commission classification code: EC 1.1.3.4) and catalase (CAT, from *bovine* liver, catalog number C40, EC 1.11.1.6) were purchased from Sigma-Aldrich (St. Louis, MO), and nitrate reductase (NR, from *Arabidopsis thaliana*, catalog number AtNaR, EC 1.7.1.1) was acquired from NECi (Lake Linden, MI). The EC number,

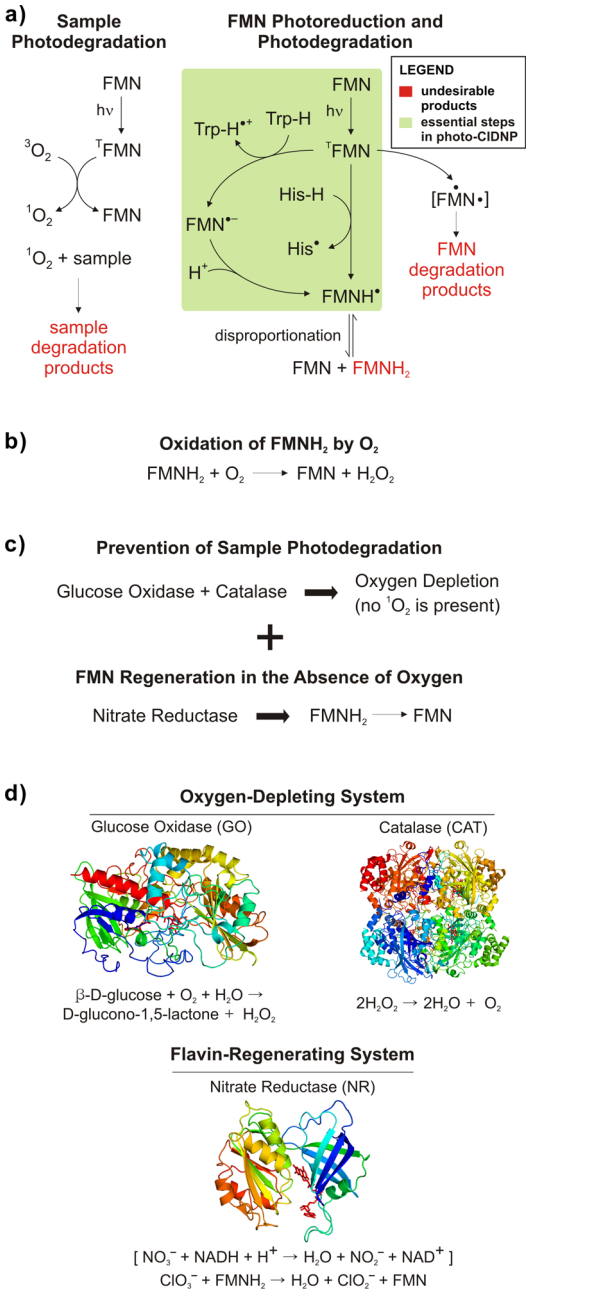

Figure 1. Diagrams illustrating the fundamental challenges underlying the enhancement of NMR signal-to-noise via photo-CIDNP, together with an outline of how the proposed tri-enzyme system meets the challenges. (a) Major pathways leading to essential processes (enclosed in the green box) and undesired products (shown in red) in photo-CIDNP NMR. The species shown in square brackets is a putative biradical intermediate in the FMN photodegradation pathway.[33] (b) Scheme showing that an advantageous feature of ambient oxygen is its ability to convert $FMNH_2$ back to FMN.[34] (c) Proposed strategy for simultaneously overcoming NMR sample photodegradation and regenerating FMN in the presence of the NR-GO-CAT tri-enzyme system. (d) Structure of the proposed photo-CIDNP-enhancing enzymes: glucose oxidase (GO, PDB ID: 1GAL), catalase (CAT, PDB ID: 1TGU), and nitrate reductase (NR, PDB ID: 2CND), together with the reactions catalyzed by each enzyme. The FAD-binding domain of *Zea mays* nitrate reductase is displayed here (instead of the *Arabidopsis thaliana* nitrate reductase, NR, used in this work) due to the lack of structural information on NR. The two enzymes have the same biological function and share considerable sequence similarity (71%). The process in square

dx.doi.org/10.1021/jp4010168 | J. Phys. Chem. B 2013, 117, 6069−6081

Figure 1. continued

brackets is the physiologically relevant NR reaction. Although both nitrate (NO_3^-) and chlorate (ClO_3^-) ions are viable substrates for NR, only ClO_3^- was used in this work.

established by the Enzyme Commission, provides an unambiguous numerical classification of enzymes based on the source organism and the reactions they catalyze. All enzymes, provided in freeze-dried form, were separately dissolved in 30 mM potassium phosphate (pH 7.0). The GO and CAT stock solution concentrations were 6.3 and 8.0 μM, respectively. The NR stock solution concentration was 10 units/mL, with one unit defined as the amount of enzyme that reduces 1.0 μmol of nitrate to nitrite per min at pH 7.5 and 30 °C, with NADH serving as the substrate. The enzyme solutions were aliquoted and flash-frozen in liquid N_2 and stored at −80 °C. Aliquots were thawed in a water bath at 30 °C before use.

NMR Sample Preparation. Trp (574597), Tyr (607991), His (608009), and FMN (F8399) were purchased from Sigma-Aldrich. The σ^{32} peptide and the N-terminal SH3 domain of the drk adaptor protein from *Drosophila melanogaster* (drkN SH3) were prepared as previously described.[20] All NMR samples contained 0.2 mM FMN and 5% D_2O. The aromatic amino acid NMR samples were in 10 mM potassium phosphate (pH 7.0) and had 0.25 μM, 0.16 μM, and 2.5 mM GO, CAT, and D-glucose (158968, Sigma-Aldrich) concentrations,[39,40] respectively, and 0.54 μM (i.e., 0.3 units per 700 μL) NR concentration.[41] NR was used in combination with 2 mM sodium chlorate (244147, Sigma-Aldrich). The σ^{32} peptide samples were in 50 mM Tris, 5 mM $MgCl_2$, and 100 mM KCl (pH 7.5), and the drkN SH3 protein samples were in 50 mM Tris, 5 mM $MgCl_2$, and 50 mM KCl (pH 7.2). Both samples had a 10-fold smaller concentration of GO and CAT and a 3-fold smaller concentration of NR. Enzyme substrate (i.e., D-glucose, sodium chlorate) concentrations were identical to those of the aromatic amino acid samples. The aromatic amino acid and σ^{32} peptide samples were incubated in the NMR spectrometer for at least 15 min and 1 h, respectively, to ensure optimal oxygen depletion prior to photo-CIDNP NMR data collection.

Photo-CIDNP Setup. An argon ion laser (2017-AR, Spectra-Physics - Newport Corporation, Irvine, CA) in multiline mode (main lines at 488 and 514 nm) was used as a light source for all photo-CIDNP experiments. The laser light was focused into an optical fiber as described,[24] using a convex lens (LB4330, Thorlabs, Newton, NJ) and a fiber-coupler (F-91-C1-T, Newport Corporation). The optical fiber was guided into the NMR sample tube via a coaxial insert (WGS-5BL, Wilmad-Labglass, Buena, NJ). The position of the coaxial insert was adjusted such that the tip of the fiber was located 5 mm above the receiver coil region. Laser powers were measured at the sample end of the optical fiber. The laser-to-fiber coupling efficiency[42] was ∼50%.

Photo-CIDNP NMR Experiments. All NMR data were collected at 25 °C on a Varian INOVA 600 MHz NMR spectrometer equipped with a triple resonance $^1H\{^{13}C, ^{15}N\}$ triple-axis gradient probe. The constant evolution time in the indirect dimension was set to 13 ms for both the ^{13}C-PRINT and SE-HSQC experiments. All the 1D data were apodized with a 5 Hz exponential line-broadening function and zero-filled twice. The 2D data were apodized with an unshifted Gaussian function and zero-filled twice in both dimensions. The relaxation delay was 10 s. The laser irradiation time was 0.1 s. The laser irradiation power was 1.5 and 0.5 W for the 1D and 2D experiments, respectively.

Determination of $(S/N)_t$ and Cumulative S/N. The signal-to-noise per unit time $(S/N)_t$ was evaluated as described.[24] Briefly, the NMR signal (S) was determined by measuring the intensity of the NMR resonance of interest relative to the average noise line. Peak-to-peak noise amplitude (N_{PTP}) was evaluated within a 4 ppm spectral width centered around the resonance of interest. The following equations were used

$$S/N = \frac{2.5 \times S}{N_{PTP}} \tag{1}$$

and

$$(S/N)_t = \frac{S/N}{\sqrt{t}} \tag{2}$$

where t is the total data collection time.[43] Note that the terms sensitivity and $(S/N)_t$ are intended to have identical meaning and are interchangeably used throughout this work. In the case of low-micromolar control SE-HSQC, the signal was so weak that prolonged data acquisition had to be carried out until a reasonable S/N was attained, to compute $(S/N)_t$. The cumulative S/N in Figure 4 was evaluated from

$$S/N = \frac{2.5 \times \sum_{i=1}^{n} S_i}{\sqrt{\sum_{j=1}^{n} N_{PTP,j}^{\ 2}}} \tag{3}$$

where n denotes the experiment number, S_1, S_2, ..., S_n are the intensities of the signal of interest across different experiments, and $N_{PTP,1}$, $N_{PTP,2}$, ..., $N_{PTP,n}$ are the corresponding peak-to-peak noise amplitudes.

ESI Mass Spectrometry. Electrospray ionization (ESI) mass spectrometry studies were carried out with the 3200 Q TRAP LC/MS/MS System (Applied Biosystems, Foster City, CA) in positive ion mode. The buffer components of all samples were removed by treatment with $ZipTip_{C18}$ devices (standard bed format, EMD Millipore Corporation, Billerica, MA). To remove low-molecular-weight impurities while preserving as much of the weakly binding Trp on the C18 column as possible, the manufacturer's recommended procedure was modified as follows. Briefly, the $ZipTip_{C18}$ was subject to (a) 3× treatment with 100% acetonitrile, (b) 30× treatment with 5% methanol/0.1% TFA in water, (c) 10× treatment with 0.1% TFA in water, (d) sample binding to the resin by multiple up/down pipetting of 30 μL of the NMR sample solution containing 0.1% TFA, (e) resin washing upon 10× treatment with 0.1% TFA in water, and (f) sample elution upon multiple up/down pipetting steps with 5 μL of 20% acetonitrile/0.1% TFA in water.

Absorption Spectroscopy in the UV−Visible Region. Absorption spectra of the NMR samples were acquired directly in the NMR tube with an HP 8452A diode array spectrophotometer. In order to properly position the NMR sample for absorption measurements, an NMR-tube cap was glued to the bottom of a disposable absorption cuvette appropriate for data collection at λ > 300 nm (14-955-129, Fisher Scientific, Pittsburgh, PA). The NMR sample was then inserted in the device, and the interstitial space between the cuvette and the NMR tube was then filled with water. Complete conversion of FMN to $FMNH_2$ was accomplished

dx.doi.org/10.1021/jp4010168 | J. Phys. Chem. B 2013, 117, 6069−6081

in a control experiment upon adding trace amounts of $Na_2S_2O_4$ (157953, Sigma-Aldrich) to a solution containing 0.2 mM FMN, 0.2 mM Trp, and 10 mM potassium phosphate at pH 7.0. Absorption data were smoothed via the boxcar averaging procedure with a 4 nm window, using the MATLAB software package (Mathworks, Natick, MA).

RESULTS AND DISCUSSION

Design of a Tri-enzyme System for Efficient Photo-CIDNP under Low-Photodegradation Conditions. Sample photodegradation upon laser irradiation is a major challenge in photo-CIDNP, which renders this technique poorly suited to long-term NMR data collection. Oxygen-dependent pathways are a prominent cause of sample photodegradation (Figure 1a).[30,31] Hence, we depleted ambient oxygen via the oxygen scavenging enzymes glucose oxidase and catalase[44] (Figure 1c and d). The GO and CAT enzymes were previously employed to deplete oxygen in fluorescence microscopy[45] but not in NMR. We favor this method over alternative mechanical procedures (usually based on flushing the system with an inert gas)[46] because it is operationally easier, more efficient, and it enables continuous oxygen depletion. Our earlier efforts based on an alternative oxygen scavenging enzyme system, protocatechuate-3,4-dioxygenase in the presence of protocatechuic acid,[47] were not further pursued because protocatechuic acid significantly quenches photo-CIDNP.

In addition to promoting undesirable sample photodegradation, O_2 is also known to mediate an important, useful purpose in photo-CIDNP, i.e., reoxidation of the dye (Figure 1b). Therefore, in addition to depleting oxygen via GO and CAT, we had to introduce an O_2 substitute capable of efficiently oxidizing the photo-CIDNP byproduct $FMNH_2$ back to FMN, without quenching ^{T}FMN. Our initial efforts focused on strong chemical oxidants. The best performing agents, Co(III) and persulfate, were able to oxidize $FMNH_2$ similarly to ambient oxygen but exhibited undesired solution behavior.

Next, we reasoned that a redox-active enzyme taking up $FMNH_2$ as a specific substrate may more effectively serve our purpose. Toward this goal, we initially tested xanthine oxidase and FMN reductase. We found, however, that neither of them is effective at oxidizing $FMNH_2$, as both enzymes thermodynamically favor the conversion of FMN to $FMNH_2$ and not vice versa. In addition, xanthine oxidase was used in the presence of urate as a substrate. However, urate weakly quenches photo-CIDNP. After some initial moderately successful attempts with nitrate reductase from *Pichia pastoris*, we selected nitrate reductase from *Arabidopsis thaliana* (NR, Figure 1c and d) due to its superior performance. The primary biological function of this enzyme is to reduce nitrate to nitrite while oxidizing NADH to NAD+.[38] Fortunately, $FMNH_2$ is also a viable substrate of the NR enzyme *in vitro*.[38] Similarly, nitrate was replaced by chlorate[48] which turned out to be more efficient at oxidizing $FMNH_2$ than nitrate. The complete reaction scheme adopted here is shown in Figure 1d.

In summary, our strategy has been to enzymatically remove molecular oxygen and concurrently reoxidize $FMNH_2$ (Figure 1c). Our tri-enzyme system, denoted here as NR-GO-CAT, consists of glucose oxidase (GO), catalase (CAT), and nitrate reductase (NR) (Figure 1d), and it successfully accomplishes the desired task. The addition of catalytic amounts of NR-GO-CAT enzymes to NMR samples leads to a significant reduction in sample photodegradation and preservation of photo-CIDNP efficiency over a much longer time span than enzyme-free solutions.

Efficient Photo-CIDNP at Low Sample Concentration (200 μM) in the Presence of the Tri-enzyme System. The effect of the NR-GO-CAT tri-enzyme system depends critically on the concentration of the target biomolecule. We began by examining 200 μM ^{15}N,^{13}C-Trp, i.e., a model compound at a concentration typically employed in biomolecular NMR. Arrays of 20 ^{13}C-PRINT spectra (^{1}H-detected ^{13}C photo-CIDNP)[20] were acquired back-to-back employing a high-power Ar ion laser (1.5 W) to examine the variation in photo-CIDNP under light conditions in the absence and presence of different combinations of enzymes (Figure 2b). Photoexcited triplet FMN converts molecular oxygen, $^3O_2$, usually present at ca. 0.27 mM in aqueous solution,[49] to singlet oxygen ($^1O_2$). The latter, in turn, causes significant sample degradation according to the scheme in Figure 1a. In order to estimate the extent of photodegradation, ^{1}H 1D pulse-acquire data were also collected before and after the array of photo-CIDNP experiments, as shown in Figure 2c.

In the absence of enzymes or in the presence of NR alone, a significant decrease in the Trp ^{13}C-PRINT resonance intensities is observed (Figure 2b). This result is a direct consequence of sample photodegradation, as illustrated in Figure 2c, showing the disappearance of most Trp signals after the photo-CIDNP experimental array, under no-enzyme and NR conditions.

In the presence of catalytic amounts of the oxygen-scavenging enzymes GO (0.25 μM) and CAT (0.16 μM), however, much higher photo-CIDNP resonance intensities are observed (Figure 2b). Figure 2c provides evidence for the origin of this effect by showing that GO and CAT prevent Trp photodegradation, as most of the Trp resonances preserve their original intensity at the end of the experiment. Hence, oxygen depletion prevents sample photodegradation and enables the photo-CIDNP S/N enhancement to persist for many transients.

The prevention of Trp photodegradation is a clear advantage. However, it is not sufficient to enable long-term photo-CIDNP data collection because, under GO-CAT conditions, the ^{13}C-PRINT intensity decreases fairly rapidly over time (Figure 2b). This phenomenon limits the ability to exploit the photo-CIDNP sensitivity enhancement in long experiments. Visual analysis of NMR samples after photo-CIDNP reveals that the solution loses a considerable fraction of its yellow color, imparted by FMN. This effect can be ascribed to either the accumulation of the nearly colorless FMN-reduction product, $FMNH_2$, expected after multiple rounds of photo-CIDNP, or irreversible FMN photodegradation (Figure 1a). Absorption spectroscopy, performed directly on the NMR samples before and after laser irradiation (Figure 3), helps to shed light on this topic.

The FMN absorption spectral changes observed after photo-CIDNP in the presence of the GO-CAT enzymes suggest that a significant fraction of FMN has been converted into other species (Figure 3b). The 344 nm isosbestic point of the pre- and post-photo-CIDNP spectra of Figure 3b (similar to the isosbestic point of FMN and $FMNH_2$ observed in the literature)[36] is consistent with the presence of both FMN and $FMNH_2$ in the post-photo-CIDNP sample. The $FMNH_2$ reference spectrum (Figure 3, dotted lines) also naturally (i.e., in agreement with the published spectrum)[36] extrapolates to this isosbestic point. Note that the $FMNH_2$ reference spectrum is not explicitly shown at wavelengths lower than 400 nm, due to overlap with the absorption band of sodium dithionite,

dx.doi.org/10.1021/jp4010168 | J. Phys. Chem. B 2013, 117, 6069−6081

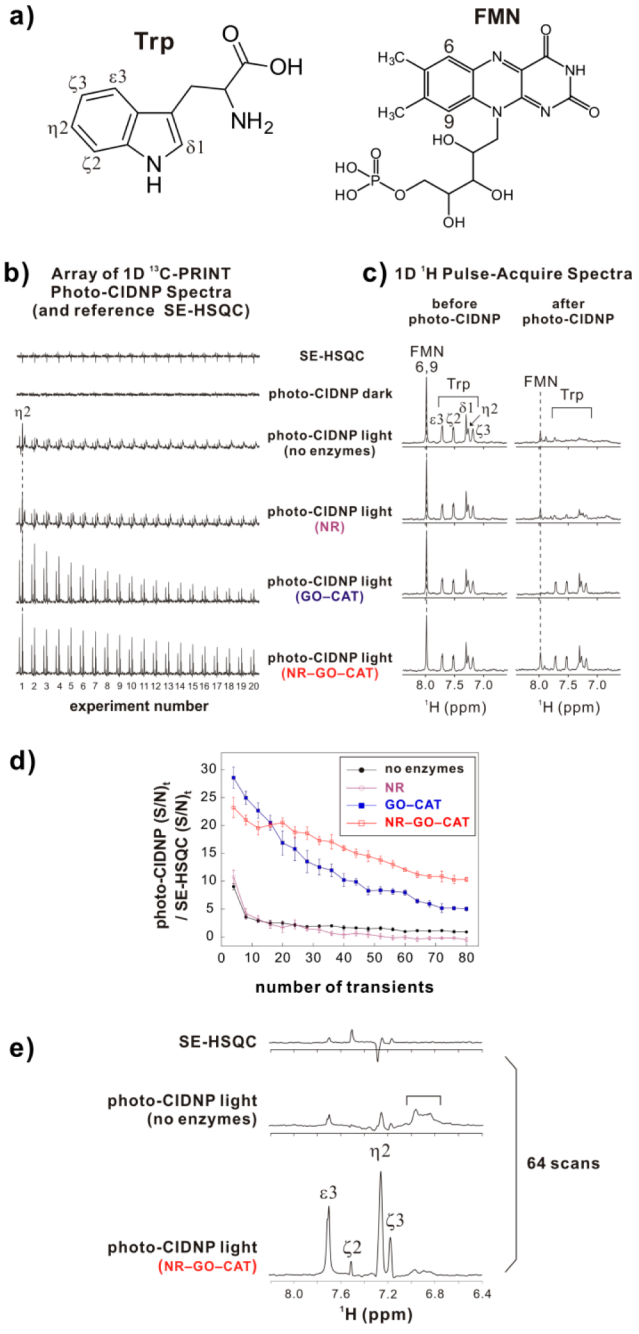

Figure 2. Laser-driven photo-CIDNP NMR of 200 μM aqueous Trp in the absence and presence of different enzymes. (a) Structure of tryptophan (Trp) and flavin mononucleotide (FMN). (b) Array of ^{1}H-detected ^{13}C-PRINT photo-CIDNP spectra in the absence and presence of different enzyme combinations (4 scans per experiment, data collected back-to-back, 80 scans total, 1.5 W laser power, 0.1 s laser pulse per scan). This panel also includes ^{1}H–^{13}C SE-HSQC reference spectra (equal number of scans and identical relaxation delay to ^{13}C-PRINT). The resonances detectable under no-enzyme and NR-only conditions are mostly due to photodegradation products. (c) ^{1}H spectra before and after the collection of the array of experiments displayed in panel b. (d) Graph illustrating the ratio of $(S/N)_t$ for ^{13}C-PRINT (light conditions) and SE-HSQC experiments (η2 Trp resonance) in the absence and presence of different enzyme combinations. Error bars denote standard errors for three independent experiments. (e) 1D ^{13}C-PRINT photo-CIDNP spectra (64 scans per spectrum) in the absence and presence of the NR-GO-CAT tri-enzyme system. The bracket in the photo-CIDNP light (no enzymes) spectrum denotes photodegradation products.

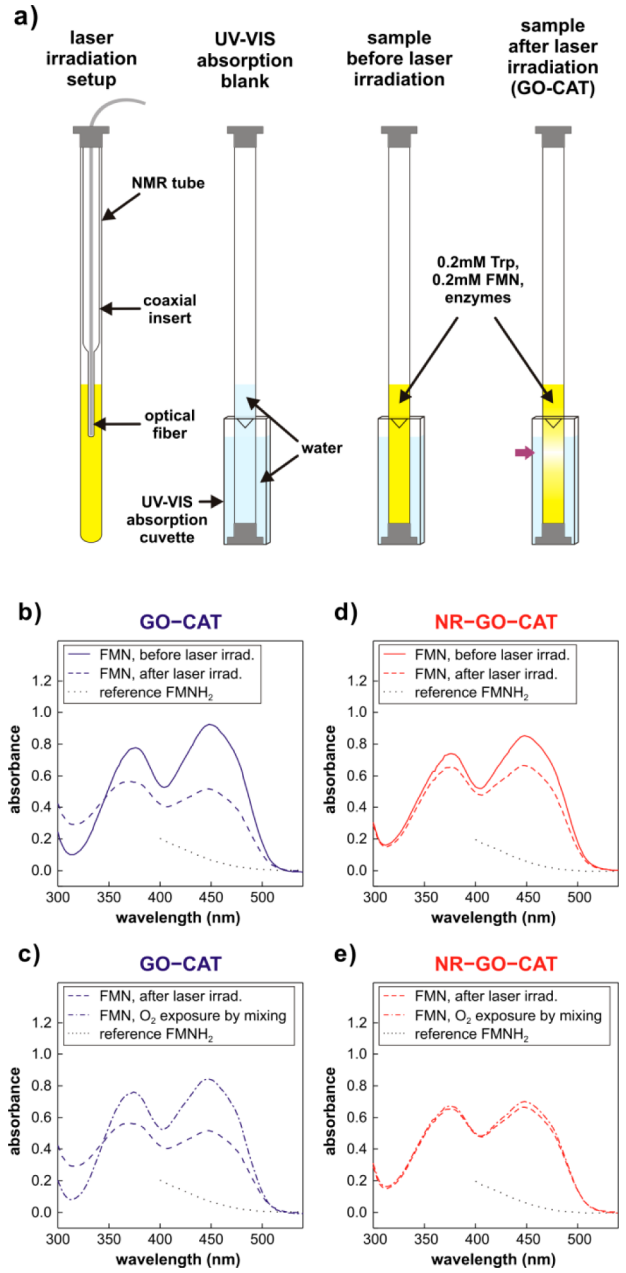

Figure 3. Electronic absorption spectroscopy of photo-CIDNP samples. (a) Experimental setup to record the absorption spectra of NMR samples directly in the NMR sample tube. The purple arrow denotes the photobleached volume (centered approximately in the region sampled by the NMR transmitter/receiver coils and the absorption spectroscopy excitation beam). FMN spectra before and after laser irradiation are plotted for (b) GO-CAT and (d) NR-GO-CAT conditions. Note that the $FMNH_2$ spectrum is shown only in the long-wavelength range due to strong absorbance by $Na_2S_2O_4$ (which was used to reduce FMN to $FMNH_2$) at short wavelength range. Absorption spectra of NMR samples after the photo-CIDNP experiments under (c) GO-CAT and (e) NR-GO-CAT conditions, before and after exposure to O_2 via sample mixing.

which was introduced in the reference sample to quantitatively convert FMN to $FMNH_2$. Transient exposure of the post-photo-CIDNP sample to molecular oxygen via manual mixing causes regeneration of FMN from $FMNH_2$, as evidenced by the spectral changes in Figure 3c. This regeneration (Figure 3c) is likely slightly overestimated, since O_2 exposure upon mixing

dx.doi.org/10.1021/jp4010168 | J. Phys. Chem. B 2013, 117, 6069–6081

inevitably involves mixing of the irradiated sample region with the nonirradiated region containing intact FMN. The same argument applies to NR-GO-CAT conditions (Figure 3e).

Incidentally, NMR (Figure 2c) suggests that FMN has been fully depleted, after the photo-CIDNP array in the presence of GO and CAT (Figure 2c, see disappearance of FMN 6 and 9 NMR resonances). However, absorption spectroscopy implies that some FMN is left in solution under the same conditions (Figure 3b). This apparent inconsistency can be explained upon considering that line broadening beyond detection of the FMN 6 and 9 overlapping ^{1}H NMR resonances is likely due to chemical exchange with trace amounts of the FMNH$^{\bullet}$ radical (Figure 1a),[50] an obligatory species in photo-CIDNP (see further comments below).

The above combined evidence highlights two important facts. First, the nearly quantitative regeneration of FMN in Figure 3c speaks in favor of long-term photo-CIDNP opportunities in the presence of NR-GO-CAT. Second, in order to perform long-term photo-CIDNP, a strategy to oxidize $FMNH_2$ *in situ* and produce FMN in the absence of molecular oxygen is necessary to further improve upon the GO-CAT conditions.

More persistent photo-CIDNP enhancements are observed when catalytic amounts (0.54 μM) of the third enzyme, NR, capable of oxidizing $FMNH_2$ back to FMN, are added to the solution. The latter conditions, including all three enzymes, are denoted here as NR-GO-CAT, and define the tri-enzyme system proposed in this study. NR-GO-CAT enables efficient photo-CIDNP (a) by synergistically minimizing the amount of sample photodegradation via GO and CAT, as shown in Figure 2c, and (b) by reoxidizing the $FMNH_2$ dye due to the specific oxidizing action of NR. The regeneration of FMN under NR-GO-CAT conditions is testified by the post-photo-CIDNP ^{1}H NMR spectrum of Figure 2c, which shows partially recovered FMN 6 and 9 resonances (with a 43 ± 5% line broadening due to chemical exchange with FMNH$^{\bullet}$ on the fast T_2 time scale) even after many photo-CIDNP cycles. The FMN recycling under NR-GO-CAT conditions is also supported by the absorption data of Figure 3d. Here, the post-photo-CIDNP FMN transition centered at ca. 400 nm is closer to the intensity before the laser irradiation, indicating that more FMN is in solution than under GO-CAT conditions (Figure 3b). The incomplete FMN recovery under NR-GO-CAT conditions is likely due to a small extent of irreversible FMN photodegradation (see also the mass spectrometry data in Figure S1, Supporting Information). The absence of an isosbestic point in Figure 3d supports the absence of $FMNH_2$ in solution. Interestingly, panel e of Figure 3 shows that upon exposure to molecular oxygen no additional intensity is recovered, indicating that the FMN regeneration ability of the NR enzyme is as good as that of molecular oxygen.

The power of the NR-GO-CAT tri-enzyme system is best recapitulated by the plot of Figure 2d, which shows the sensitivity of ^{13}C-PRINT in the presence of NR-GO-CAT relative to the sensitivity of the reference ^{1}H−^{13}C SE-HSQC. The data show that ^{13}C-PRINT in the presence of the tri-enzyme system is more sensitive than ^{1}H−^{13}C SE-HSQC by up to 25-fold. In addition, the NR-GO-CAT photo-CIDNP experiments are dramatically, i.e., up to 13 ± 2 times, more effective than enzyme-free photo-CIDNP, even after collection of many transients.

The slightly smaller ratio of $(S/N)_t$ observed for NR-GO-CAT (red trace in Figure 2d) relative to GO-CAT (blue trace in Figure 2d) during the initial ~15 scans is likely due to the EDTA in the commercially available NR source.[15] The secondary substrate of NR, sodium chlorate (2 mM), which is also added to the solution, does not have a significant effect on photo-CIDNP.

Figure 2e provides a visual illustration of the results achievable in a single relatively long-term experiment (64 scans) in the absence and presence of the NR-GO-CAT enzyme system. Only the latter photo-CIDNP experiment leads to minimal (<10%) photodegradation. The advantages of photo-CIDNP in the presence of the tri-enzyme system over SE-HSQC and regular enzyme-free photo-CIDNP are evident.

The effect of the argon ion laser power on photo-CIDNP experiments carried out in the presence and absence of the tri-enzyme system is shown in Figure 4. For all the powers tested

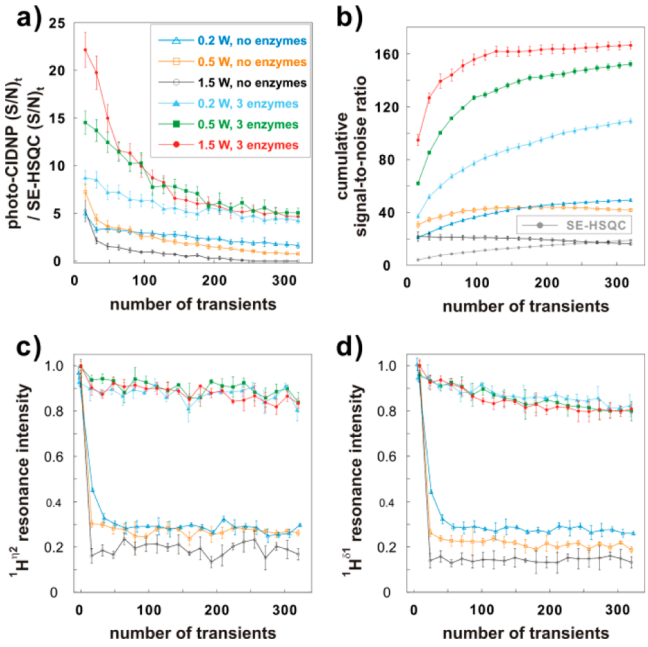

Figure 4. Effect of laser power and long-term photo-CIDNP data collection on 200 μM Trp in the absence and presence of the NR-GO-CAT enzymes. (a) Ratio of ^{13}C-PRINT (light conditions) and ^{1}H−^{13}C SE-HSQC $(S/N)_t$ values for the η2 Trp resonance, as successive experiments were run on the same sample. Photo-CIDNP experiments were run at variable laser powers. Twenty successive data sets, comprising 16 scans each, were collected for each trace shown. (b) Cumulative S/N for the η2 Trp resonance under different experimental conditions. This plot was generated from the data in panel a. Variations in (c) η2 and (d) δ1 ^{1}H Trp resonance intensities during photo-CIDNP experiments in panel a. ^{1}H and photo-CIDNP (panel a) data were collected in an interleaved fashion. Error bars denote standard errors for three independent experiments. Note that the amount of sample preservation under no-enzyme conditions is overestimated in panels c and d, given that the $^{1}H^{\eta 2}$, $^{1}H^{\delta 1}$ Trp resonances after the laser irradiations were on top of a blob in the ^{1}H spectra, which most likely arises from the photodegradation products (Figure 2c).

(0.2, 0.5, and 1.5 W), the NR-GO-CAT-containing samples perform much better than the samples lacking the enzymes. At the highest laser power (1.5 W), the NR-GO-CAT system is particularly effective, highlighting the usefulness of the three enzymes under conditions yielding the largest NMR sensitivity. Panel b of Figure 4, which provides cumulative S/N values, is particularly useful at illustrating this point. At 1.5 W and 320

dx.doi.org/10.1021/jp4010168 | J. Phys. Chem. B 2013, 117, 6069−6081

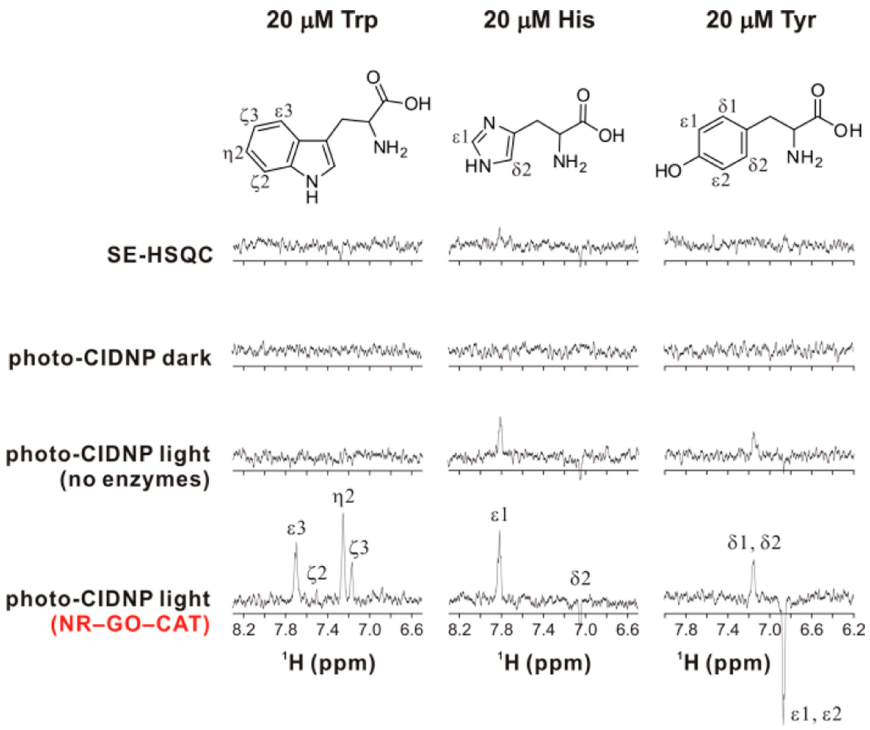

Figure 5. ^{13}C-PRINT photo-CIDNP and reference ^{1}H−^{13}C SE-HSQC of Trp, His, and Tyr at 20 μM concentration in the absence and presence of the tri-enzyme system (16 scans/experiment). Photo-CIDNP data under light conditions were collected at 1.5 W laser power with 0.1 s laser pulse/scan.

transients, the overall S/N of the sample containing NR-GO-CAT is ca. 8-fold larger than in the no-enzyme and control SE-HSQC cases.

In order to quantitatively characterize the extent of sample photodegradation during photo-CIDNP, ^{1}H pulse-acquire and ^{13}C-PRINT photo-CIDNP data were collected in an interleaved fashion. In the presence of the tri-enzyme system, regardless of laser power, sample integrity is preserved by >80%, even after 320 laser pulses, as shown in panels c and d of Figure 4. Hence, it is generally advantageous to use the three-enzyme system for photo-CIDNP experiments at high Ar ion laser power.

Extending the Applicability of the Tri-enzyme System to Other Amino Acids and Polypeptides at Even Lower Concentration (20 μM). To probe the effectiveness of the tri-enzyme system at even lower sample concentration and with more diverse NMR samples, we investigated three aromatic amino acids (Trp, His, and Tyr) and the σ^{32} peptide[20] at 20 μM concentration.

For all the aromatic amino acids, we could only observe distinct resonances when the photo-CIDNP experiments were carried out in the presence of the three enzymes (Figure 5). The SE-HSQC, photo-CIDNP dark (i.e., laser off), and enzyme-free photo-CIDNP light spectra yielded very little or no signal. The ratios of the $(S/N)_t$ of the photo-CIDNP resonances in the presence of NR- GO-CAT over the corresponding values for the SE-HSQC control are 24, 5, and 14 for Trp, His, and Tyr, respectively. The extent of photodamage, defined as the variation in ^{1}H resonance intensity (in ^{1}H 1D pulse-acquire experiments) before and after the photo-CIDNP arrays (Figure 5) is moderate, <5%, for Trp, His, and Tyr in the presence of NR-GO-CAT.

Next, we tested the σ^{32} peptide, which comprises 13 amino acids (i.e., residues 132−144) of the *E. coli* σ^{32} transcription factor. This peptide, which is known to be a high-affinity client of the DnaK *E. coli* chaperone,[51] was modified by replacing Leu_{135} with ^{13}C, ^{15}N-Trp (Figure 6a).[20] 1D ^{13}C PRINT photo-CIDNP experiments in the presence of NR-GO-CAT displayed a 25-fold greater $(S/N)_t$ than the reference ^{1}H−^{13}C-SE-HSQC experiment (Figure 6b). This is a significant increase in sensitivity, which amounts to a 625-fold faster data collection than in the case of SE-HSQC.

The extent of σ^{32} peptide photodegradation was estimated by acquiring a 1D ^{1}H−^{13}C SE-HSQC spectrum before and after the photo-CIDNP light experiments (in this case, 1D ^{1}H pulse-acquire experiments were not appropriate to estimate photodegradation due to excessive resonance overlap). The extent of detected peptide photodegradation was minimal (<5%, assessed from the variation in Trp resonance intensities).

Finally, to illustrate that the combined use of photo-CIDNP and the tri-enzyme system facilitates multidimensional spectroscopy at high sensitivity, we acquired 2D ^{13}C-PRINT spectra of the 20 μM σ^{32} peptide. As shown in Figure 6c, the spectral quality is excellent, and the data show once again that the only sample yielding any detectable signal, at this very low peptide concentration, is the tri-enzyme-containing σ^{32} solution. The effectiveness of the tri-enzyme system is not limited to amino acids and peptides, and is also evident in larger molecular systems including proteins. The 2D ^{13}C-PRINT photo-CIDNP NMR spectra of the 20 μM drkN SH3 protein (~7 kDa) in the absence and presence of the tri-enzyme system, shown in Figure S2 (Supporting Information), illustrate this point.

Stretching the Concentration Limits down to 5 μM. We probed whether photo-CIDNP in combination with the tri-enzyme system may lower typical NMR sample concentrations even further down to the low μM range (we tested 5 μM). This concentration is around 2 orders of magnitude smaller than concentrations conventionally used in biomolecular NMR.

dx.doi.org/10.1021/jp4010168 | J. Phys. Chem. B 2013, 117, 6069−6081

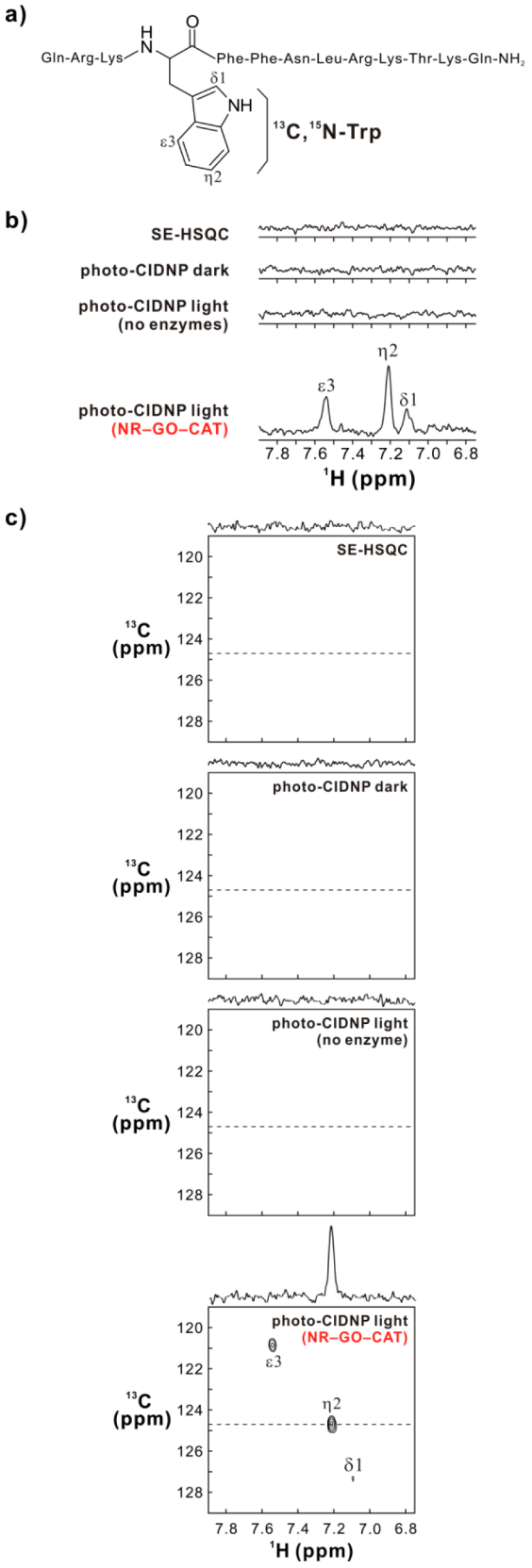

Figure 6. 1D and 2D ^{13}C-PRINT photo-CIDNP spectra of diluted σ^{32} peptide (20 μM) in the absence and presence of the NR-GO-CAT tri-enzyme system. (a) Structure of the σ^{32} peptide. (b) 1D ^{13}C-PRINT and reference ^{1}H–^{13}C SE-HSQC spectra. Photo-CIDNP under light conditions was carried out at 1.5 W laser power with 0.1 s laser pulse irradiation time with and without the NR-GO-CAT enzymes. Each experiment consisted of 32 scans. (c) 2D ^{13}C-PRINT and reference ^{1}H–^{13}C SE-HSQC spectra. Data were collected according to STATES-TPPI with 32 increments and 1 scan per increment. Spectral widths were 6000 and 4000 Hz for the direct and indirect dimensions, respectively. A 0.5 W laser power and a 0.1 s laser pulse irradiation time were employed. The dashed lines indicate the position of the 1D ^{1}H spectral slices displayed on top of each 2D spectrum.

We tested the tri-enzyme system in the presence of increasingly lower concentrations of the σ^{32} peptide (200, 20, and 5 μM). Strikingly, we observed larger relative sensitivity enhancements (with respect to SE-HSQC) at lower sample concentrations (Figure 7). The relative sensitivity enhancement reaches 48.0 ± 5.6-fold in the case of the 5 μM σ^{32} peptide (see Figure 7c for NMR spectra of this sample), corresponding to a 2304-fold reduction in data collection time, relative to SE-HSQC, as illustrated in Figure 7b.

To explain this interesting phenomenon, we performed kinetic simulations (see details in the Supporting Information text) and showed that the concentration of the $Trp^{\bullet+}$ $FMN^{\bullet-}$ radical ion pair, which is a precursor for photo-CIDNP, is predicted to decrease nonlinearly as the Trp concentration decreases. However, this decrease occurs to a much smaller extent than the decrease in sensitivity of the reference SE-HSQC, thus explaining the experimentally observed trends of Figure 7a. Similar arguments are likely to apply to other photo-CIDNP substrates than Trp. Note that concentration-dependent phenomena similar to those observed here were previously observed at acidic and basic pH,[52−54] and explained on the basis of degenerate electron exchange. At the neutral pH studied here, degenerate electron exchange is not expected to play a significant role, and the above radical-ion-pair population arguments best explain our results.

Efficient Photo-CIDNP at High Sample Concentration (5 mM). Photo-CIDNP experiments whose goal is either fast data collection of a soluble target (i.e., kinetic studies) or the identification of solvent exposure of selected amino acids[55,56] do not require data collection at very low sample concentration. In this case, photo-CIDNP experiments are often performed at high concentrations, e.g., in the mM range or higher. Even within this concentration regime, the tri-enzyme system provides key advantages. However, the balance between the different chemical paths (Figure 1a) varies dramatically when sample concentration (in this case 5 mM) exceeds both dye (usually 0.2 mM) and ambient oxygen concentration (~0.27 mM), as detailed below.

The behavior of the tri-enzyme system at high sample concentration was tested on Trp (5 mM) upon collecting ^{13}C-PRINT spectral arrays in the absence and presence of enzymes, as shown in Figure 8. Once again, we find that enzyme additives are essential to guarantee long-term data collection. Surprisingly, however, the benefits can be ascribed primarily to the NR enzyme. This statement is justified by the fact that the NR and NR-GO-CAT conditions yield substantially identical enhancements (Figure 8). If anything, the presence of GO and CAT has a deleterious effect on the initial spectral enhancement, as seen upon comparing the GO-CAT and no-enzyme conditions (Figure 8). This is due to efficient FMN conversion to $FMNH_2$ at high sample concentration (Figure 1a). The latter species, in turn, is not reoxidized by oxygen in the presence of GO and CAT. In summary, at high sample concentration, the O_2

dx.doi.org/10.1021/jp4010168 | J. Phys. Chem. B 2013, 117, 6069−6081

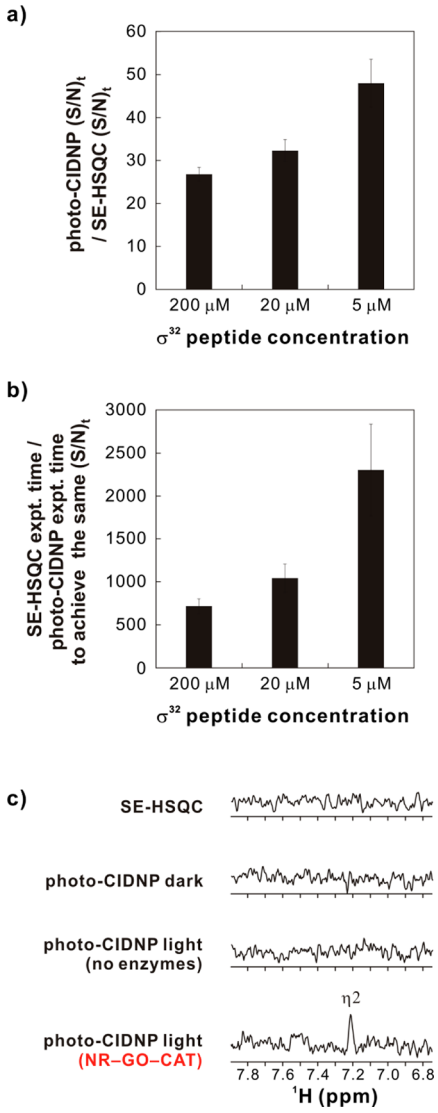

Figure 7. Improvement in laser-driven NMR sensitivity at low sample concentrations. (a) Block diagram illustrating the ratio of $(S/N)_t$ of 1D ^{13}C-PRINT (light NR-GO-CAT conditions, 16 scans, 1.5 W 0.1 s laser pulses) and 1D ^{1}H–^{13}C SE-HSQC for the σ^{32} peptide (Trp η2 resonance) at increasingly low concentration. Photo-CIDNP and control SE-HSQC experiments were performed at the same peptide concentration. In the case of the reference 1D ^{1}H–^{13}C SE-HSQC experiment, data were averaged over 128, 3072, and 14 336 scans for 200, 20, and 5 μM concentration samples, respectively, in order to achieve measurable S/N. Even after 14 336 scans, however, since S/N was poor for the 5 μM sample, the 20 μM sample SE-HSQC $(S/N)_t$ was divided by 4 and used as a reference for the 5 μM ^{13}C-PRINT experiment. Three independent experiments were performed at each concentration. (b) The time required for SE-HSQC to achieve the same sensitivity as photo-CIDNP at different sample concentrations was calculated from panel a. (c) ^{13}C-PRINT photo-CIDNP experiments on the σ^{32} peptide in the absence and presence of the tri-enzyme system at extremely low peptide concentration (5 μM). All data were collected with 16 scans, and 1.5 W, 0.1 s laser pulses were employed under light conditions.

depletion accomplished by GO and CAT is not crucial for sensitivity enhancement purposes.

Our data show that at 5 mM Trp concentration the fraction of Trp photodegradation in the absence of enzymes is small (Figure S3, Supporting Information), indeed much smaller than

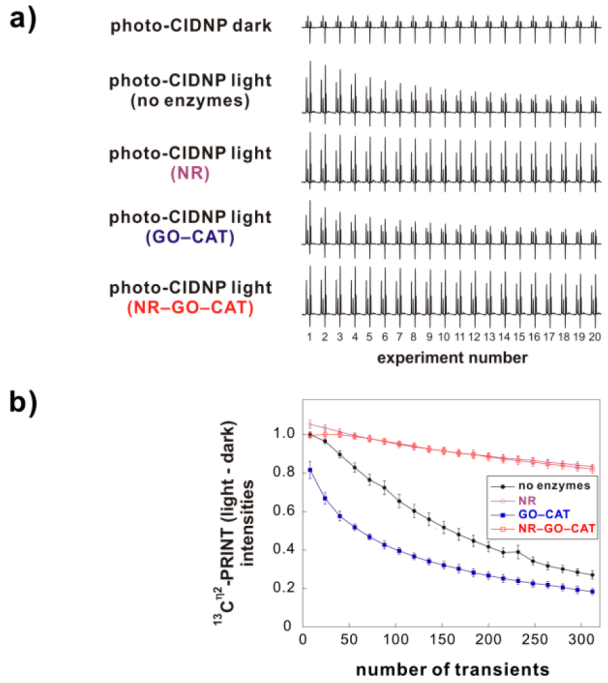

Figure 8. Photo-CIDNP NMR of aqueous Trp at high concentration (5 mM) in the absence and presence of different enzymes. (a) Spectral arrays illustrating ^{1}H-detected ^{13}C-PRINT photo-CIDNP data (16 scans per spectrum) collected back-to-back in the absence and presence of enzymes. Photo-CIDNP data under light conditions were collected with 1.5 W laser power and 0.1 s laser pulse irradiation. (b) Plot illustrating the difference between ^{13}C-PRINT photo-CIDNP signal intensities under light (i.e., laser on) and dark (i.e., laser off) conditions for the Trp η2 resonance. Three independent data sets were collected.

at 200 μM sample concentration (e.g., compare Figures 2c and S3 (Supporting Information)). Given that sample photodegradation is mediated primarily by singlet oxygen (Figure 1a), the small extent of photodegradation explains why oxygen depletion via GO and CAT is not necessary. Now, it is important to ask why sample photodegradation is not an issue at high concentrations.

Two arguments help here. First, the equilibrium concentration of dissolved oxygen in aqueous solution, in the absence of oxygen-scavenging agents, is ca. 0.27 mM.[49] Even if all the oxygen molecules were totally committed to photodegradation, the fraction of sample photodegradation would be only 5.4%. Upon considering that oxygen diffuses into the receiver-coil-sensitive region of the NMR-tube solution very slowly in the absence of mixing (see details in the Supporting Information text), very low oxygen-dependent sample photodegradation is expected for samples whose concentration is much greater than 0.27 mM. Second, Figure 1a shows that both oxygen-dependent sample photodegradation and photo-CIDNP (i.e., the steps in the green box) proceed via the key reaction intermediate ^{T}FMN. According to our simulation (Supporting Information text), at higher sample concentration, the ^{T}FMN population is significantly lower. Hence, it is straightforward to appreciate that high NMR sample concentrations lead to the depletion of most ^{T}FMN in solution, significantly decreasing the rate of oxygen-mediated sample photodegradation.

Mass action arguments related to the high Trp concentration (Figure 1a) explain why most FMN undergoes photoreduction to $FMNH_2$, instead of irreversible decomposition. Hence, the

dx.doi.org/10.1021/jp4010168 | J. Phys. Chem. B 2013, 117, 6069–6081

NR enzyme is maximally effective under these conditions, as shown in Figure 8. Indeed, NR is the key enzyme at high sample concentration, and the effect of NR alone is entirely similar to that of the NR-GO-CAT combination (Figure 8). In addition, a comparison between no-enzyme and NR-GO-CAT conditions (Figure 8) illustrates the fact that NR has higher oxidizing power compared to that of oxygen.

Under both NR and NR-GO-CAT conditions, a moderate decrease in resonance intensity is observed over long-term data collection (Figure 8b). Figure S3 (Supporting Information) shows that this decrease is qualitatively consistent with a small extent of oxygen-dependent sample photodegradation. This undesired effect can be minimized upon collecting data under GO-CAT conditions, though the lack of NR reduces the signal-enhancement benefits of photo-CIDNP (Figure 8b). The moderate extent of sample photodegradation (<10%) observed after extensive data collection under NR or NR-GO-CAT conditions cannot currently be overcome. On the other hand, these conditions are advantageous because they yield remarkable signal enhancements over a prolonged time scale.

Identity of FMN Photodegradation Products after Prolonged Laser Irradiation. A comparison between Figures 4a and 8a (at 1.5 W laser power) in the absence of enzymes shows that photo-CIDNP is more amenable to the collection of multiple scans when the sample concentration is high. To explain the origin of this phenomenon, we performed ESI mass spectrometry before and after the photo-CIDNP experiments of Figures 4a and 8a (320 scans, 1.5 W, 0.1 s laser pulse/scan, no enzymes, see Figure 9). Although the ESI data are not entirely quantitative due primarily to the different ionization efficiencies of the species involved and to the uneven affinities of the different compounds to the C_{18} reverse-phase desalting pipet tip (used during sample preparation for mass spectrometry), the method provides semiquantitative information on the species involved, including the identity of any FMN photodegradation products generated upon extensive high power FMN laser irradiation. Given the mass spectrometry sample preparation conditions, which involve extensive exposure to oxygen, any $FMNH_2$ present in the samples is reversibly oxidized back to FMN. Hence, ESI mass spectrometry is mostly suitable to follow the formation of irreversible photodegradation products, rather than assessing the FMN/$FMNH_2$ balance.

The results in Figure 9 show that FMN (originally present at 0.2 mM concentration) is no longer present in the low-concentration (0.2 mM) Trp samples, while it is distinctly observable at higher Trp concentration (5 mM), after 320 high-power (1.5 W) laser pulses. These data demonstrate that FMN experiences a larger extent of irreversible photodegradation at low Trp concentrations. The above results can be explained on the basis of the reaction diagram in Figure 1a. At high Trp concentration, the photochemically generated ^{T}FMN follows the green photo-CIDNP pathway due to the mass action of Trp, while at low Trp concentration the FMN irreversible photodegradation pathway dominates.

Finally, ESI mass spectrometry enables assessing the molecular identity of some of the FMN irreversible degradation products, which can be identified from their m/z values (Figure 9a–e). Consistent with the literature,[32] the low-concentration Trp samples subject to extensive laser irradiation contain both lumichrome (LC, Figure 9f) and formyllumiflavin (FLF, Figure 9f) as the primary FMN degradation products. This result does not exclude that other FMN degradation products undetectable by mass spectrometry (e.g., due to their high molecular weight, poor ionization properties, or nonuniform efficiency in the desalting process) may also be present.

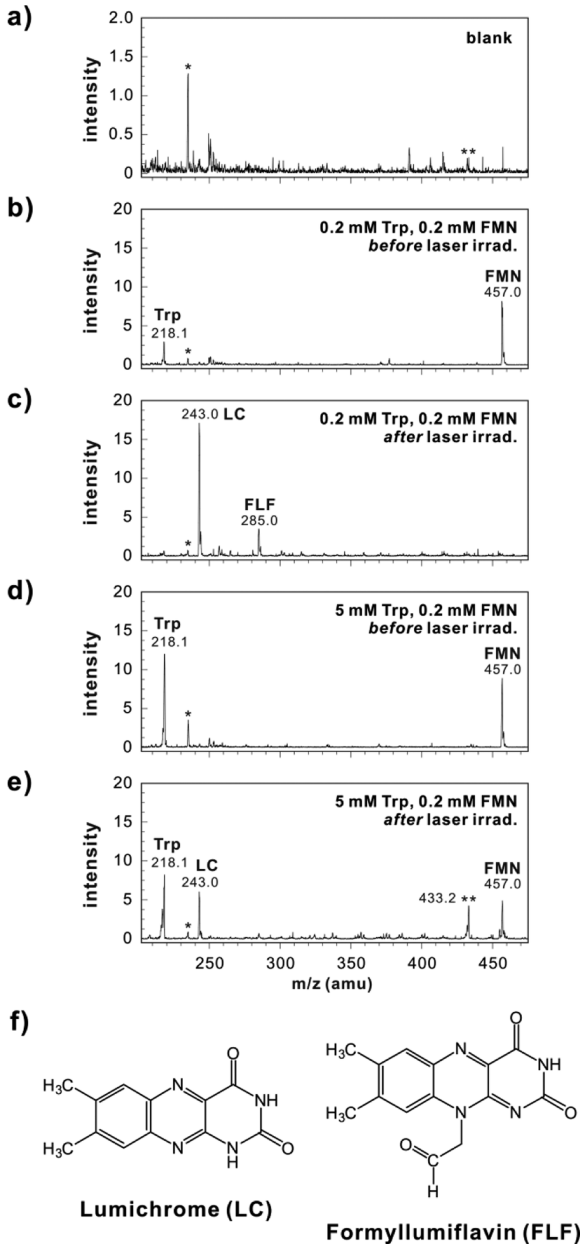

Figure 9. Electrospray ionization (ESI) mass spectra of samples containing Trp and FMN before and after 1D $^{1}H-^{13}C$ SE-HSQC (320 scans, light conditions, 1.5 W laser, 0.1 s laser pulse/scan) experiments. (a) Control blank experiment on desalted buffer. Note that the vertical scale of this plot is 10-fold smaller than that in all the other plots. (b, c) 0.2 mM Trp. (d, e) 5 mM Trp. The symbol * denotes peaks that are also observed in the blank. The symbol ** denotes a peak that is unidentified but is also observed in the blank at low intensity. (f) Structure of the FMN photodegradation products LC and FLF. Note that the FMN peak represents both FMN and $FMNH_2$ species, since $FMNH_2$ is oxidized to FMN during the mass spectrometry sample preparation.

Alternative Strategies and Future Perspectives. The quest to prevent undesired processes mediated by either singlet oxygen or the triplet excited state of the dye is shared by techniques other than NMR. For instance, fluorescence microscopy and spectroscopy, which often employ high-

dx.doi.org/10.1021/jp4010168 | J. Phys. Chem. B 2013, 117, 6069–6081

power laser sources, have witnessed a variety of advances targeting the suppression of irreversible photodegradation and reversible fluorophore transition to dark states (blinking). To gain a wider perspective, it is useful to compare the features of our tri-enzyme system with those of the popular antibleaching/antidegradation agents used in fluorescence. The oxygen-scavenging system GO-CAT[44] or protocatechuate-3,4-dioxygenase,[47] for instance, are sometimes employed in fluorescence, either alone or in combination with the small molecules TROLOX[57] and ROXS.[58] The latter two agents act by similar principles.[59] ROXS, for instance, contains a mixture of oxidizing and reducing agents that efficiently depopulate triplet excited states of the dye and convert them back to the singlet ground state via redox chemistry. This effect minimizes reversible fluorophore blinking and irreversible photodegradation. TROLOX, ROXS, or variations thereof, however, cannot be employed in photo-CIDNP given that they deplete triplet excited states. Photo-CIDNP, on the other hand, exploits the long lifetime of triplet excited states, so that productive collisions between ^{T}FMN and the target photo-CIDNP-active molecule generate triplet radical-pair intermediates. In summary, TROLOX and ROXS overcome photodegradation and blinking in fluorescence but are not appropriate for use in photo-CIDNP.

Oxygen depletion has long been known to prolong the triplet-excited-state lifetimes of dyes.[60] This effect is expected to intrinsically benefit photo-CIDNP, and may be partially responsible for the observed sensitivity enhancements in the presence of the GO and CAT enzymes.

Although all photo-CIDNP experiments in this work were performed by ^{1}H-detected ^{13}C photo-CIDNP,[20] the tri-enzyme system is to be considered generally applicable to all other photo-CIDNP experiments.[24,25] In addition to its general applicability, another advantageous feature of NR-GO-CAT is the fact that these enzymes are effective at very low concentrations, in the sub-μM range. Hence, they are minimally perturbative to the system of interest.

In light of the above, what are the future challenges to further photo-CIDNP performance especially at low sample concentrations, where sensitivity improvements are most sorely needed? As much as it is good news that photo-CIDNP sensitivity increases at low sample concentration in the presence of NR-GO-CAT (Figure 7), the extent of FMN photodegradation increases at low sample concentrations (Figure 9). Overcoming the latter effect will be the goal for future developments in this area.

CONCLUSIONS

High sensitivity is crucial in many biomolecular NMR applications. This study introduces a novel tri-enzyme system that dramatically enhances photo-CIDNP performance in the presence of high-power laser irradiation, enhancing the ability to achieve high S/N in NMR. At low-mM concentrations, which have been commonly used in biomolecular photo-CIDNP applications to date, efficient long-term photo-CIDNP data collection is achieved thanks to the extremely efficient FMN-recycling ability of the NR enzyme. Under these conditions, sample photodegradation is minimized in the presence of the GO and CAT enzymes.

Further, at sample concentrations in the low-μM range (where photo-CIDNP experiments could not be performed before), even greater sensitivity enhancements were observed in the presence of the NR-GO-CAT enzymes. For instance, at 5 μM σ^{32} peptide sample concentration, 48-fold larger sensitivity than SE-HSQC was reached with a 2304-fold savings in data collection time. In summary, our results contribute to render photo-CIDNP a general, desirable methodology to analyze NMR samples containing different types of aromatic amino acids at extremely high sensitivity in solution.

ASSOCIATED CONTENT

Supporting Information

Supporting text and figures describing (i) the computational prediction of radical ion pair and triplet-excited-state FMN (^{T}FMN) populations during continuous-wave laser irradiation and (ii) photodegradation profiles under different conditions are provided. This material is available free of charge via the Internet at http://pubs.acs.org.

AUTHOR INFORMATION

Corresponding Author

*Phone: 608-262-5430. Fax: 608-262-9918. E-mail: cavagnero@chem.wisc.edu.

Notes

The authors declare no competing financial interest.

ACKNOWLEDGMENTS

We thank Charlie Fry, Yusuke Okuno, Steve Burke, and John Wright for useful discussions. We are also grateful to Yusuke Okuno for a critical reading of the manuscript. This research was funded by the National Institute of Health grant R21AI088551.

REFERENCES

(1) Overhauser, A. W. Polarization of Nuclei in Metals. *Phys. Rev.* **1953**, *92*, 411−415.

(2) Maly, T.; et al. Dynamic Nuclear Polarization at High Magnetic Fields. *J. Chem. Phys.* **2008**, *128*, 052211.

(3) Griesinger, C.; Bennati, M.; Vieth, H. M.; Luchinat, C.; Parigi, G.; Hofer, P.; Engelke, F.; Glaser, S. J.; Denysenkov, V.; Prisner, T. F. Dynamic Nuclear Polarization at High Magnetic Fields in Liquids. *Prog. Nucl. Magn. Reson. Spectrosc.* **2012**, *64*, 4−28.

(4) Ardenkjaer-Larsen, J. H.; Fridlund, B.; Gram, A.; Hansson, G.; Hansson, L.; Lerche, M. H.; Servin, R.; Thaning, M.; Golman, K. Increase in Signal-to-Noise Ratio of >10,000 Times in Liquid-State NMR. *Proc. Natl. Acad. Sci. U.S.A.* **2003**, *100*, 10158−10163.

(5) Lee, Y.; Zeng, H.; Mazur, A.; Wegstroth, M.; Carlomagno, T.; Reese, M.; Lee, D.; Becker, S.; Griesinger, C.; Hilty, C. Hyperpolarized Binding Pocket Nuclear Overhauser Effect for Determination of Competitive Ligand Binding. *Angew. Chem., Int. Ed.* **2012**, *51*, 5179−5182.

(6) Natterer, J.; Bargon, J. Parahydrogen Induced Polarization. *Prog. Nucl. Magn. Reson. Spectrosc.* **1997**, *31*, 293−315.

(7) Theis, T.; Ganssle, P.; Kervern, G.; Knappe, S.; Kitching, J.; Ledbetter, M. P.; Budker, D.; Pines, A. Parahydrogen-Enhanced Zero-Field Nuclear Magnetic Resonance. *Nat. Phys.* **2011**, *7*, 571−575.

(8) Spence, M. M.; Rubin, S. M.; Dimitrov, I. E.; Ruiz, E. J.; Wemmer, D. E.; Pines, A.; Yao, S. Q.; Tian, F.; Schultz, P. G. Functionalized Xenon as a Biosensor. *Proc. Natl. Acad. Sci. U.S.A.* **2001**, *98*, 10654−10657.

(9) Navon, G.; Song, Y.; Room, T.; Appelt, S.; Taylor, R. E.; Pines, A. Enhancement of Solution NMR and MRI with Laser-Polarized Xenon. *Science* **1996**, *271*, 1848−1848.

(10) Haupt, J. A New Effect of Dynamic Polarization in a Solid Obtained by Rapid Change of Temperature. *Phys. Lett. A* **1972**, *38*, 389−390.

(11) Bargon, J.; Fischer, H.; Johnson, U. Nuclear Magnetic Resonance Emission Lines during Fast Radical Reactions. I. Recording Methods and Examples. *Z. Naturforsch., A* **1967**, *22*, 1551−1555.
(12) Ward, H. R.; Lawler, R. G. Nuclear Magnetic Resonance Emission and Enhanced Absorption in Rapid Organometallic Reactions. *J. Am. Chem. Soc.* **1967**, *89*, 5518−5519.
(13) Cocivera, M. Optically Induced Overhauser Effect in Solution. Nuclear Magnetic Resonance Emission. *J. Am. Chem. Soc.* **1968**, *90*, 3261−3263.
(14) Kaptein, R.; Dijkstra, K.; Nicolay, K. Laser Photo-CIDNP as a Surface Probe for Proteins in Solution. *Nature* **1978**, *274*, 293−294.
(15) Hore, P. J.; Broadhurst, R. W. Photo-CIDNP of Biopolymers. *Prog. Nucl. Magn. Reson. Spectrosc.* **1993**, *25*, 345−402.
(16) Goez, M. Photo-CIDNP Spectroscopy. In *Annual Reports on NMR Spectroscopy*; Webb, G. A., Ed.; Academic Press: London, 2009; Vol. *66*, pp 77−147.
(17) Morozova, O. B.; Ivanov, K. L.; Kiryutin, A. S.; Sagdeev, R. Z.; Köchling, T.; Vieth, H. M.; Yurkovskaya, A. V. Time-Resolved CIDNP: an NMR Way to Determine the EPR Parameters of Elusive Radicals. *Phys. Chem. Chem. Phys.* **2011**, *13*, 6619−6627.
(18) Kaptein, R.; Oosterhoff, J. L. Chemically Induced Dynamic Nuclear Polarization II - (Relation with Anomalous ESR Spectra). *Chem. Phys. Lett.* **1969**, *4*, 195−197.
(19) Closs, G. L.; Closs, L. E. Induced Dynamic Nuclear Spin Polarization in Photoreductions of Benzophenone by Toluene and Ethylbenzene. *J. Am. Chem. Soc.* **1969**, *91*, 4549−4550.
(20) Lee, J. H.; Sekhar, A.; Cavagnero, S. 1H-Detected 13C Photo-CIDNP as a Sensitivity Enhancement Tool in Solution NMR. *J. Am. Chem. Soc.* **2011**, *133*, 8062−8065.
(21) Daviso, E.; Janssen, G. J.; Alia, A.; Jeschke, G.; Matysik, J.; Tessari, M. A 10,000-Fold Nuclear Hyperpolarization of a Membrane Protein in the Liquid Phase via Solid-State Mechanism. *J. Am. Chem. Soc.* **2011**, *133*, 16754−16757.
(22) Zysmilich, M. G.; McDermott, A. Photochemically Induced Dynamic Nuclear Polarization in the Solid-State 15N Spectra of Reaction Centers from Photosynthetic Bacteria *Rhodobacter sphaeroides* R-26. *J. Am. Chem. Soc.* **1994**, *116*, 8362−8363.
(23) Lyon, C. E.; Jones, J. A.; Redfield, C.; Dobson, C. M.; Hore, P. J. Two-Dimensional 15N-1H Photo-CIDNP as a Surface Probe of Native and Partially Structured Proteins. *J. Am. Chem. Soc.* **1999**, *121*, 6505−6506.
(24) Sekhar, A.; Cavagnero, S. 1H Photo-CIDNP Enhancements in Heteronuclear Correlation NMR Spectroscopy. *J. Phys. Chem. B* **2009**, *113*, 8310−8318.
(25) Sekhar, A.; Cavagnero, S. EPIC- and CHANCE-HSQC: Two 15N Photo-CIDNP-Enhanced Pulse Sequences for the Sensitive Detection of Solvent-Exposed Tryptophan. *J. Magn. Reson.* **2009**, *200*, 207−213.
(26) Kiryutin, A. S.; Korchak, S. E.; Ivanov, K. L.; Yurkovskaya, A. V.; Vieth, H. M. Creating Long-Lived Spin States at Variable Magnetic Field by Means of Photochemically Induced Dynamic Nuclear Polarization. *J. Phys. Chem. Lett.* **2012**, *3*, 1814−1819.
(27) Goez, M.; Kuprov, I.; Hore, P. J. Increasing the Sensitivity of Time-Resolved Photo-CIDNP Experiments by Multiple Laser Flashes and Temporary Storage in the Rotating Frame. *J. Magn. Reson.* **2005**, *177*, 139−145.
(28) Kurt, N.; Rajagopalan, S.; Cavagnero, S. Effect of Hsp70 Chaperone on the Folding and Misfolding of Polypeptides Modeling an Elongating Protein Chain. *J. Mol. Biol.* **2006**, *355*, 809−820.
(29) Rajagopalan, S.; Kurt, N.; Cavagnero, S. High-Resolution Conformation and Backbone Dynamics of a Soluble Aggregate of Apomyoglobin119. *Biophys. J.* **2011**, *100*, 747−755.
(30) Connolly, P. J.; Hoch, J. C. Photochemical Degradation of Tryptophan Residues during CIDNP Experiments. *J. Magn. Reson.* **1991**, *95*, 165−173.
(31) Pattison, D. I.; Davies, M. J. Actions of Ultraviolet Light on Cellular Structures. *EXS* **2006**, *96*, 131−157.
(32) Holzer, W.; Shirdel, J.; Zirak, P.; Penzkofer, A.; Hegemann, P.; Deutzmann, R.; Hochmuth, E. Photo-Induced Degradation of Some Flavins in Aqueous Solution. *Chem. Phys.* **2005**, *308*, 69−78.
(33) Moore, W. M.; Spence, J. T.; Raymond, F. A.; Colson, S. D. Photochemistry of Riboflavin. I. The Hydrogen Transfer Process in the Anaerobic Photobleaching of Flavins. *J. Am. Chem. Soc.* **1963**, *85*, 3367−3372.
(34) Müller, F., Ed. *Chemistry and Biochemistry of Flavoenzymes*; CRC Press: Boca Raton, FL, 1991.
(35) Maeda, K.; Lyon, C. E.; Lopez, J. J.; Cemazar, M.; Dobson, C. M.; Hore, P. Improved Photo-CIDNP Methods for Studying Protein Structure and Folding. *J. Biomol. NMR* **2000**, *16*, 235−244.
(36) Song, S. H.; Dick, B.; Penzkofer, A. Photo-Induced Reduction of Flavin Mononucleotide in Aqueous Solutions. *Chem. Phys.* **2007**, *332*, 55−65.
(37) Scheek, R. M.; Stob, S.; Boelens, R.; Dijkstra, K.; Kaptein, R. Applications of Two-Dimensional 1H Nuclear Magnetic Resonance Methods in Photochemically Induced Dynamic Nuclear Polarisation Spectroscopy. *Faraday Discuss. Chem. Soc.* **1984**, *78*, 245−256.
(38) Campbell, W. H. Nitrate Reductase Structure, Function and Regulation: Bridging the Gap Between Biochemistry and Physiology. *Annu. Rev. Plant Physiol. Plant Mol. Biol.* **1999**, *50*, 277−303.
(39) Swoboda, B. E. P.; Massey, V. Purification and Properties of the Glucose Oxidase from *Aspergillus niger*. *J. Biol. Chem.* **1965**, *240*, 2209−2215.
(40) Yousefi, R.; Saboury, A. A.; Ghadermarzi, M.; Moosavi-Movahedi, A. A. Effects of Cysteine on the Inactivation of Bovine Liver Catalase. *Bull. Korean Chem. Soc.* **2000**, *21*, 567−570.
(41) Skipper, L.; Campbell, W. H.; Mertens, J. A.; Lowe, D. J. Pre-Steady-State Kinetic Analysis of Recombinant Arabidopsis NADH:Nitrate Reductase: Rate-Limiting Processes in Catalysis. *J. Biol. Chem.* **2001**, *276*, 26995−27002.
(42) Wirmer, J.; Kuhn, J.; Schwalbe, H. Millisecond Time Resolved Photo-CIDNP NMR Reveals a Non-Native Folding Intermediate on the Ion-Induced Refolding Pathway of Bovine Alpha-Lactalbumin. *Angew. Chem., Int. Ed.* **2001**, *40*, 4248−4251.
(43) Ernst, R. R.; Bodenhausen, G.; Wokaun, A. *Principles of Nuclear Magnetic Resonance in One and Two Dimensions*; Oxford University Press: Upper Saddle River, NJ, 1989.
(44) Benesch, R. E.; Benesch, R. Enzymatic Removal of Oxygen for Polarography and Related Methods. *Science* **1953**, *118*, 447−448.
(45) Roy, R.; Hohng, S.; Ha, T. A Practical Guide to Single-Molecule FRET. *Nat. Methods* **2008**, *5*, 507−516.
(46) Englander, S. W.; Calhoun, D. B.; Englander, J. J. Biochemistry without Oxygen. *Anal. Biochem.* **1987**, *161*, 300−306.
(47) Aitken, C. E.; Marshall, R. A.; Puglisi, J. D. An Oxygen Scavenging System for Improvement of Dye Stability in Single-Molecule Fluorescence Experiments. *Biophys. J.* **2008**, *94*, 1826−1835.
(48) Barber, M. J.; Notton, B. A. Spinach Nitrate Reductase: Effects of Ionic Strength and pH on the Full and Partial Enyzyme Activities. *Plant Physiol.* **1990**, *93*, 537−540.
(49) Murov, S. L.; Carmichael, I.; Hug, G. L. *Handbook of Photochemistry*; Marcel Dekker: New York, 1993.
(50) Ehrenberg, A.; Müller, F.; Hemmerich, P. Basicity, Visible Spectra, and Electron Spin Resonance of Flavosemiquinone Anions. *Eur. J. Biochem.* **1967**, *2*, 286−293.
(51) McCarty, J. S.; Rüdiger, S.; Schönfeld, H. J.; Schneider-Mergener, J.; Nakahigashi, K.; Yura, T.; Bukau, B. Regulatory Region C of the *E. coli* Heat Shock Transcription Factor, Sigma32, Constitutes a DnaK Binding Site and Is Conserved among Eubacteria. *J. Mol. Biol.* **1996**, *256*, 829−837.
(52) Tsentalovich, Y. P.; Morozova, O. B.; Yurkovskaya, A. V.; Hore, P. J. Kinetics and Mechanism of the Photochemical Reaction of 2,2′-Dipyridyl with Tryptophan in Water: Time-Resolved CIDNP and Laser Flash Photolysis Study. *J. Phys. Chem. A* **1999**, *103*, 5362−5368.
(53) Tsentalovich, Y. P.; Morozova, O. B. Laser Flash Photolysis and Time Resolved CIDNP Study of Photoreaction of 2,2′-Dipyridyl with N-Acetyl Tyrosine in Aqueous Solutions. *J. Photochem. Photobiol., A* **2000**, *131*, 33−40.

(54) Tsentalovich, Y. P.; Morozova, O. B.; Yurkovskaya, A. V.; Hore, P.; Sagdeev, R. Z. Time-Resolved CIDNP and Laser Flash Photolysis Study of the Photoreactions of N-Acetyl Histidine with 2,2′-Dipyridyl in Aqueous Solution. *J. Phys. Chem. A* **2000**, *104*, 6912−6916.
(55) Mok, K. H.; Kuhn, L. T.; Goez, M.; Day, I. J.; Lin, J. C.; Andersen, N. H.; Hore, P. J. A Pre-Existing Hydrophobic Collapse in the Unfolded State of an Ultrafast Folding Protein. *Nature* **2007**, *447*, 106−109.
(56) Buck, F.; Ruterjans, H.; Kaptein, R.; Beyreuther, K. Photochemically Induced Dynamic Nuclear Polarization Investigation of Complex Formation of the NH2-Terminal DNA-Binding Domain of Lac Repressor with Poly[d(AT)]. *Proc. Natl. Acad. Sci. U.S.A.* **1980**, *77*, 5145−5148.
(57) Rasnik, I.; McKinney, S. A.; Ha, T. Nonblinking and Long-Lasting Single-Molecule Fluorescence Imaging. *Nat. Methods* **2006**, *3*, 891−893.
(58) Vogelsang, J.; Kasper, R.; Steinhauer, C.; Person, B.; Heilemann, M.; Sauer, M.; Tinnefeld, P. A Reducing and Oxidizing System Minimizes Photobleaching and Blinking of Fluorescent Dyes. *Angew. Chem., Int. Ed.* **2008**, *47*, 5465−5469.
(59) Cordes, T.; Vogelsang, J.; Tinnefeld, P. On the Mechanism of Trolox as Antiblinking and Antibleaching Reagent. *J. Am. Chem. Soc.* **2009**, *131*, 5018−5019.
(60) Ha, T.; Tinnefeld, P. Photophysics of Fluorescent Probes for Single-Molecule Biophysics and Super-Resolution Imaging. *Annu. Rev. Phys. Chem.* **2012**, *63*, 595−617.